Distributed Online Energy Management in Interconnected Microgrids

Hualei Zou, *Student Member, IEEE*, Yu Wang, *Member, IEEE*, Shiwen Mao, *Fellow, IEEE*, Fanghua Zhang, and Xin Chen, *Member, IEEE*

***Abstract*—In this article, a hierarchical online distributed algorithm (HODA) is developed to achieve optimal energy management in interconnected microgrids (IMG). The energy management objectives include maximizing users' utility, optimizing the output power of controllable generators, and keeping the system operating in an economic manner. We formulate the problem as an online least absolute shrinkage and selection operator (LASSO) problem, considering both reactive power and system operation characteristics. We then employ averaging fixed horizon control (AFHC) to solve the formulated problem under some mild assumptions on the uncertainties in renewable power generation and load demand. The alternating direction method of multipliers (ADMM) is adopted to decouple the coupled constraints. The proposed online algorithm is asymptotically optimal, since its solution converges to the offline optimal solution. The performance of the proposed algorithm is validated using data traces obtained from a real-world IMG system.**

***Index Terms*—Alternating direction method of multipliers (ADMM), distributed energy management, interconnected microgrids (IMG), online least absolute shrinkage and selection operator (LASSO).**

I. Introduction

THE SMART grid/microgrid (SG/MG) is an important domain of the Internet of Things (IoT), which aims to achieve reliable information transmission through smart facilities (e.g., smart meters), and realize real-time control, accurate management, and scientific decision making of the SG/MG by the smart devices [1], [2]. In recent years, more and more renewable resources are integrated into the SG/MG, which incorporates the techniques of data communication, energy management, and computation intelligence to provide sustainable economic and secure power supply [3]. The energy management system (EMS) for the MG is therefore extensively studied to achieve effective use of renewable energy, improvement of demand profile, optimization of the utility, and so on [4]. With the development of MG and EMS, the interconnected microgrids (IMG) has become a new trend to promote cooperation among the MGs for better system reliability and economic benefits. Usually, an IMG is composed of a cluster of MGs, which are often geographically close and connected to a distribution bus, and a significant feature of the IMG is the highly efficient utilization of renewable energy, especially distributed renewable energy (DRE) [5]–[7]. In spite of the above advantages, there are still many challenges in achieving a stable and reliable operation of IMG. The EMS in the IMG is more complex than that in an islanded MG, and the existing challenges motivate researchers to pursue better solutions.

High utilization of renewable resources and low-cost power generation in IMG have been the primary goals for new solutions to achieve resilient and highly self-healing operation of MGs [8]. The related literature [9]–[11] are focused on the cooperative power management strategies in IMG, and Wang *et al.* [3] and Rahbar *et al.* [12], [13] mainly studied the problem of energy exchanging and trading in IMG. For example, in order to find the cooperative power management strategies for IMG, the game theory has been applied to optimize the trading of renewable energy with fairness considerations [10], [11]. These studies have been able to achieve the goal of optimal energy scheduling in IMG autonomously. However, the existing works only consider the balance of supply and demand of *active power* in IMG. Several other important aspects, including the actual power flows and system operational constraints, have not been fully considered. In order to ensure the stable operation of IMG, although the adjustment of active power is very important, the role of *reactive power* and *system operation characteristics* in scheduling optimization cannot be ignored, especially in the case of renewable energy resources or large load variations [14]. In such cases, simultaneous adjusting both active and reactive power can ensure the system always provide high-quality power and stable operation, while the consideration of electrical characteristics guarantees more accurate scheduling. Motivated by this observation, some scholars have already studied the above problem. In [15], a distributed decoupling optimization algorithm for networked MGs is studied. However, this article only considers the electrical characteristics of the utility MG, but does not consider the electrical characteristics of the private MGs. As a result, such results will have limited practical significance for the private MGs.

Manuscript received September 22, 2019; revised November 12, 2019; accepted November 21, 2019. Date of publication December 3, 2019; date of current version April 14, 2020. This work was supported in part by the NSF of China under Grant 51607087; in part by the Fundamental Research Funds for the Central Universities of China under Grant XCA17003-06; in part by the NSF in part under Grant DMS-1736470; and in part by the Wireless Engineering Research and Education Center (WEREC), Auburn University, Auburn, AL, USA. *(Corresponding author: Shiwen Mao.)*

H. Zou, Y. Wang, F. Zhang, and X. Chen are with the Department of Electrical Engineering, Nanjing University of Aeronautics and Astronautics, Nanjing 210016, China (e-mail: zouhualei@nuaa.edu.cn; yuwang15@nuaa.edu.cn; zhangfh@nuaa.edu.cn; chen.xin@nuaa.edu.cn).

S. Mao is with the Department of Electrical and Computer Engineering, Auburn University, Auburn, AL 36849 USA (e-mail: smao@ieee.org).

Digital Object Identifier 10.1109/JIOT.2019.2957158

The algorithm proposed in [4] considers the system operation characteristics. However, the proposed method is only suitable for a centralized power management; the autonomous energy scheduling of each MG in the IMG cannot be realized.

In this article, a hierarchical online distributed algorithm (HODA) for IMG is proposed, which considers both *reactive power* and *system operation characteristics*. Based on the electrical characteristics of IMG, the algorithm can achieve the highest user satisfaction and realize the optimal scheduling of adjustable generators. Aiming at the coupling relationship existing in IMG, this article employs the alternating direction method of multipliers (ADMM) algorithm to enable autonomous energy distribution. Some researchers have adopted ADMM to tackle power optimization problems [15], [16]. Ma *et al.* [15] applied ADMM to IMG, and the work [16] uses ADMM to achieve optimal power flows (OPFs) in a power system. However, the ADMM algorithm cannot be directly employed to solve the problem studied in this article, due to the objective function that is nonsmooth convex, and the time-coupled variables in the objective functions.

In addition, another challenge comes from the various and strongly correlated uncertainties of renewable power generation and load demand in IMG, which complicate the energy management design. Note that the energy management is for the future (e.g., day-ahead or hour-ahead), and is thus heavily dependent on forecast values of future renewable power generations and load demands. Inaccurate predictions of power generation and load demand can cause large discrepancies between the optimal scheduling and the actual results in day-ahead scheduling [3]. So online algorithms have been recognized to be highly promising for real-time energy scheduling in power systems [3], [15], [17]. Some existing online algorithms for MG energy management, e.g., [17], are asymptotically optimal, i.e., their solution converges to the offline optimal solution. However, these studies only consider active power flows in the MGs.

Motivated by the prior works, we formulate the online energy distribution as an OPF problem with multiobjectives, which include maximizing uses' utility, optimizing (i.e., smoothing) the output power of controllable generators, and keeping the IMG system operating in an economic way. We show that the formulated problem is an online least absolute shrinkage and selection operator (LASSO) problem, and the averaging fixed horizon control (AFHC) is then employed to solve this problem under some mild assumptions on the uncertainties (i.e., forecasting errors) in renewable power generation and load demand [18]. For the strong coupled constraints as a result of the IMG topology, in order to achieve distributed energy management, ADMM is adopted to decouple the constraints [19]. For the 1-norm term in the objective functions, the soft-thresholding operator is employed to solve it directly [19], [20]. Since the power flow equality constraints are nonconvex [21], slack variables are introduced to transform the constraints to convex [22]. The proposed HODA takes into account both actual power laws and system operational constraints.

We show that the proposed HODA converges to the offline optimal solution, and the online results can achieve a sublinear regret and constant competitive ratio. To validate the performance of the proposed scheme, we apply it to a real-world IMG deployed in Hekou, Nantong City, Jiangsu Province, China. Our simulation study shows that HODA can effectively decouple the IMG constraints and achieve autonomous energy management in both the main grid and every MG. It also enables distributed optimization with greatly reduced computational complexity.

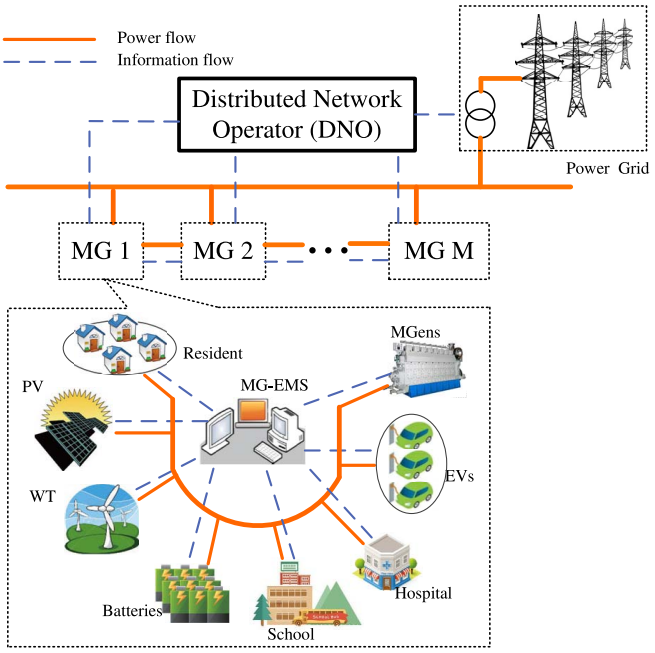

Fig. 1. System architecture of an IMG with a link connection structure.

The remainder of this article is organized as follows. We present the system model and problem statement in Section II. The proposed distributed online optimization approaches are developed and analyzed in Section III. The simulation, validation, and evaluation of our proposed algorithm are represented in Section IV. Section V concludes this article.

II. System Model and Problem Formulation

A. System Model

We consider an IMG with several interconnected MGs integrated with the main grid. There are renewable resources, energy storage system (ESS), microgenerators (MGens), diesel generators, load demand, distributed network operator (DNO), main grid EMS (M-EMS), and MG-EMS in each MG, as shown in Fig. 1. The renewable energy sources in the IMG include photovoltaic (PV), wind turbine (WT), and so on. The energy consumption in the IMG can be made by residential, commercial, and industrial consumers. Such loads are usually divided into two types [17], [23]. One type is fixed load, such as refrigerators in houses and manufacturing machines in factories. The others are elastic loads, such as electric vehicles (EVs), heating, ventilation, and air conditioning (HVAC), and washer/dryers, which can be flexibly scheduled in the IMG.

As in Fig. 1, the DNO can send commands to M-EMS and MG-EMS through communication network links. The EMS in the IMG is used to achieve the optimal energy distribution.

Both complex power and information flow bidirectionally. Moreover, the ESS charges when there is extra power and discharges when the demand is larger than the distributed generation. The elastic load is also one of the effective ways to consume excess energy to balance the supply and demand and maximize the utilization of renewable resources. Furthermore, reactive power resources, such as ESS, MGens, and static var compensator (SVC), are regulated to mitigate the voltage fluctuations at each node, which is caused by the intermittent generation of renewable energy sources and random load demand in the IMG [4]. On the basis of achieving stable operation of the system, the EMS aims to achieve the maximum user satisfaction for electricity usage. The system can operate in an economic way, and the optimal output power of the adjustable power generation can be achieved.

Let d denote the real power generation of the diesel generator, $d \in \mathcal{D} = \{1, 2, \ldots, D\}$, and $\mathcal{D}$ be the set of all diesel generators in the IMG. We define the set of active powers of ESS as $s \in \mathcal{S} = \{1, 2, \ldots, S\}$, and the elastic load as $e \in \mathcal{E} = \{1, 2, \ldots, E\}$. The set of real power resources $\mathcal{G}$ is constituted by $\mathcal{D}$, $\mathcal{S}$, and $\mathcal{E}$. Actually, distributed energy scheduling is related to the structural parameters in the IMG. In our model, the set of buses is $\mathcal{B}$, and $i, j \in \mathcal{B} = \{1, 2, \ldots, B\}$. The notation used in this article is summarized in Tables I and II.

TABLE I
NOMENCLATURE

Symbol	*Description*
T	duration of one round
t	time slot, $t = 1, 2, ..., T$
m	number of Microgrids, $m = 1, 2, ..., M$
D	total number of diesel generators in the IMG
R	total number of renewable generators in the IMG
L	total number of load demand in the IMG
B	total number of nodes in the IMG
D_μ	total number of diesel generators in the Main Grid
R_μ	total number of renewable generators in the Main Grid
L_μ	total number of load demand in the Main Grid
D_m	total number of diesel generators in MG m
R_m	total number of renewable generators in MG m
L_m	total number of load demand in MG m
i, j	indices of buses in the power system
e, f	real, imaginary parts of voltage
P	real/active power in the power system
Q	reactive power in the power system
Structure Parameters	
$G_{i,j}$	conductance between node i and j
$B_{i,j}$	susceptance between node i and j
$\alpha_{d,t}$, $\beta_{d,t}$, $\lambda_{d,t}$	cost coefficient of diesel generator d at time t in the IMG
η	diesel generator's smoothing coefficient in DSO
$\alpha^m_{d,t}$,$\beta^m_{d,t}$, $\lambda^m_{d,t}$	cost coefficient of diesel generator d at time t in MG m
η_m	diesel generator's smoothing coefficient in MG m
ω	prediction window size
$C_{d,t}$	cost of all diesel generators at time t
Sets	
$\mathcal{B}$	set of nodes in the IMG
$\mathcal{D}$	set of diesel generators in the IMG
$\mathcal{S}$	set of ESS in the IMG
$\mathcal{E}$	set of elastic load in the IMG
$\mathcal{B}_\mu$	set of buses in the Main Grid
$\mathcal{D}_\mu$	set of diesel generators in the Main Grid
$\mathcal{S}_\mu$	set of ESS in the Main Grid
$\mathcal{B}_m$	set of nodes in MG m
$\mathcal{D}_m$	set of diesel generators in MG m
$\Pi^\mu(i)$	set of nodes connected to node i, $i \in \mathcal{B}_\mu$
$\Pi^m(j)$	set of nodes connected to node j, $j \in \mathcal{B}_m$

B. Problem Formulation

1) Overall Power Scheduling Problem PROB-IMG: Jointly considering the users' satisfaction, diesel generators' output power, power generation cost, and IMG's electrical characteristics, we formulate the power scheduling problem PROB-IMG as follows:

$$\begin{aligned}\min: \quad & \sum_{t=1}^{T}\Bigg\{\Big[P_{l,t}+P_{e,t}-\big(\rho_{d,t}P_{d,t}+\rho_{s,t}P_{s,t}+\rho_{r,t}P_{r,t}\big)\Big]^2 \\ & +\sum_{m=1}^{M}\Big[P^m_{l,t}+P^m_{e,t}-\big(\rho_{d,t}P^m_{d,t}+\rho_{s,t}P^m_{s,t}+\rho_{r,t}P^m_{r,t}\big)\Big]^2 \\ & +\sum_{d=1}^{D_\mu}\eta|P_{d,t}-P_{d,t-1}| \\ & +\sum_{d=1}^{D_m}\eta_m|P^m_{d,t}-P^m_{d,t-1}|\Bigg\} \qquad (1)\end{aligned}$$

$$\text{s.t.:} \quad \sum_{d=1}^{D}\Big(\alpha_{d,t}P^2_{d,t}+\beta_{d,t}P_{d,t}+\lambda_{d,t}\Big)\le C_{d,t}. \qquad (2)$$

In (1), the first and second terms represent the dissatisfaction of users in the main grid and MGs, respectively; and the third and fourth terms denote the cost of variation in the output of diesel generator. Constraint (2) is the upper bounds on the costs of diesel generators at time t.

1) The power-flow constraints in the IMG are as follows:

$$\begin{cases} P_{g,i}-\sum_j\left[e_i(e_jG_{ij}-f_jB_{ij})+f_i(f_jG_{ij}+e_jB_{ij})\right]=P_{l,i} \\ Q_{g,i}-\sum_j\left[f_i(e_jG_{ij}-f_jB_{ij})-e_i(f_jG_{ij}+e_jB_{ij})\right]=Q_{l,i} \\ \quad i,j\in\mathcal{B} \quad \forall t \end{cases} \qquad (3)$$

where e_i and f_i are the real and imaginary parts of the voltage at bus i, respectively; $P_{l,i}$ and $Q_{l,i}$ are the active and reactive power demand at bus i, respectively; and G_{ij} and B_{ij} are the conductance and susceptance between nodes i and j, respectively. Constraint (3) aims to achieve the balance of supply and demand in both real and reactive powers, while this balance is related to the voltage of each bus and the structure parameters in the IMG.

2) The limits of active and reactive power of the distributed generators, and that of the ESS capacity is given as follows:

$$\begin{cases} P^{\min}_{g,i}\le P_{g,i}\le P^{\max}_{g,i},\ i\in\mathcal{B} \quad \forall t \\ Q^{\min}_{g,i}\le Q_{g,i}\le Q^{\max}_{g,i},\ i\in\mathcal{B} \quad \forall t \\ SoC_{s,t}=SoC_{s,t-1}-\eta_sP_{s,t},\ s\in\mathcal{S}\ \forall t \\ SoC^{\min}_s\le SoC_{s,t}\le SoC^{\max}_s,\ s\in\mathcal{S} \quad \forall t \end{cases} \qquad (4)$$

Constraint (4) is used to ensure that all the generators are operated in the safe range, and all the batteries are always operated within their capacity. This is very important to achieve stable operation in the IMG.

3) In order to keep the voltage of each bus in the IMG within the stable range, we enforce limits on the voltage

TABLE II
NOMENCLATURE (CONT'D)

Variables in the IMG	
Variables	*Description*
$P_{g,i}$	active power of generator g at node i
$Q_{g,i}$	reactive power of generator g at node i
$P_{l,i}$	active power of fixed load demand at node i
$P_{e,i}$	active power of elastic load demand at node i
$P_{r,i}$	active power of renewable power at node i
$P_{d,i}$	active power of diesel generator's output power at node i
$P_{s,i}$	active power of battery's output power at node i
$Q_{l,i}$	reactive power of load demand at node i
$Q_{e,i}$	reactive power of elastic load demand at node i
$Q_{s,i}$	reactive power of battery at node i
$Q_{r,i}$	reactive power of renewable generator at node i
$Q_{d,i}$	reactive power of generator d at node i
$\rho_{r,t}, \rho_{s,t}, \rho_{d,t}$	efficiency of the converters connected to renewable generators and ESS, and the power loss in MGENs at time t
e_i, f_i	real and imaginary part of voltage at node i
e_{ref}, f_{ref}	real and imaginary part of voltage at reference node
Variables in MGs	
Variables	*Description*
$P^m_{l,i}$	active power of fixed load demand at node i
$P^m_{e,i}$	active power of elastic load demand at node i
$P^m_{r,i}$	active power of renewable power at node i
$P^m_{d,i}$	active power of diesel generator's output power at node i
$P^m_{s,i}$	active power of battery's output power at node i
$Q^m_{l,i}$	reactive power of load demand at node i
$Q^m_{e,i}$	reactive power of elastic load demand at node i
$Q^m_{s,i}$	reactive power of battery
$Q^m_{r,i}$	reactive power of renewable generator
$Q^m_{d,i}$	reactive power of diesel
$\rho^m_{r,t}, \rho^m_{s,t}, \rho^m_{d,t}$	efficiency of the converters connected to the renewable generators and ESS, and the power loss in MGENs at time t
Variables	
$P_{net,t}$	net active power demand at time t
$SoC_{s,t}$	battery s state of charge at time t
o^{max}, o^{min}	upper, lower bound of variables
$\hat{v}$	predictive value of v
σ	decay exponent of forecasting error
$\xi_{g,i}, \gamma_{g,i}$	auxiliary variables
$\zeta^{\mu}, \zeta^{m}, \psi^{\mu}, \psi^{m}$	dual variables in the Main grid and the MGs

amplitude at each bus and the reference bus, as

$$\begin{cases} (V_i^{\min})^2 \le (e_i^2 + f_i^2) \le (V_i^{\max})^2, \ i \in \mathcal{B} \quad \forall t \\ e_{ref}^2 = e_0^2 \quad \forall t \\ f_{ref}^2 = f_0^2 \quad \forall t. \end{cases} \tag{5}$$

From (1)–(5), it can be seen that the overall objective is the nonsmooth convex function, and constraint (3) is nonconvex, which means PROB-IMG is nontrivial to solve. Furthermore, PROB-IMG can be solved unless all information of the IMG is known *a priori* for the entire time period T. Moreover, even if all the necessary past and future information is known, it is very difficult to deal with such a complex problem in practice. Actually, in a centralized manner, it is computationally intensive, time consuming, with a heavy communication burden, and with poor privacy protection. Therefore, it is desirable to manage the IMG in a distributed manner instead, with reduced computation, lower communication overhead, better privacy, and autonomous operation.

From (1)–(5), we find that the objective function and the constraints are decomposable. Thus, we decompose the problem into the main grid and the MG operation problems, which are called PROB-I and PROB-II, respectively. In PROB-I, the objective is to maximize the users' satisfaction and optimize the operation of the diesel generators in the main grid. The cost of the main grid is mainly from the diesel generators, and we assume such cost is bounded [3]. Each MG has a similar objective function. The specific mathematical models for problems PROB-I and PROB-II are given in the following.

2) PROB-I for the Main Grid: The objective function in the main grid is given by

$$\min \quad \sum_{t=1}^{T} \left\{ \left[P^{\mu}_{l,t} + P^{\mu}_{e,t} - (\rho^{\mu}_{d,t} P^{\mu}_{d,t} + \rho^{\mu}_{s,t} P^{\mu}_{s,t} + \rho^{\mu}_{r,t} P^{\mu}_{r,t}) \right]^2 + \sum_{d=1}^{D_{\mu}} \eta |P^{\mu}_{d,t} - P^{\mu}_{d,t-1}| \right\}. \tag{6}$$

The operational cost in the main grid is given by

$$\sum_{d=1}^{D_{\mu}} (\alpha^{\mu}_{d,t} (P^{\mu}_{d,t})^2 + \beta^{\mu}_{d,t} P^{\mu}_{d,t} + \lambda^{\mu}_{d,t}) \le C^{\mu}_{d,t}, d \in \mathcal{D}_{\mu} \quad \forall t. \tag{7}$$

For stable operation of the main grid, the upper and lower limits of the adjustable power generation units should be satisfied as in constraint (4), and the node voltage relationship in the main power grid should be satisfied as in constraint (5). For balancing supply and demand, constraint (3) should be satisfied for $i \in \mathcal{B}_{\mu}$. However, at the nodes connected to the main grid and the MGs, a part of the bus is located in the set of MGs, i.e., $j \in \mathcal{B}_m$. The power-flow constraints of the buses connecting to the MGs are given by

$$\begin{cases} P^{\mu}_{g,i} - \sum_j [e_i(e_j G_{ij} - f_j B_{ij}) + f_i(f_j G_{ij} + e_j B_{ij})] = P^{\mu}_{l,i} \\ Q^{\mu}_{g,i} - \sum_j [f_i(e_j G_{ij} - f_j B_{ij}) - e_i(f_j G_{ij} + e_j B_{ij})] = Q^{\mu}_{l,i} \\ i \in \mathcal{B}_{\mu}, j \in \mathcal{B}_{\mu} \cup \mathcal{M}_m \quad \forall t. \end{cases} \tag{8}$$

3) PROB-II for Each MG m: Note that some MGs are connected in the IMG. The MGs may be owned and operated by different entities, so their objectives and operation conditions should be mutually independent. The objective of an MG m is given by

$$\min: \quad \sum_{t=1}^{T} \left\{ \left[P^{m}_{l,t} + P^{m}_{e,t} - (\rho^{m}_{d,t} P^{m}_{d,t} + \rho^{m}_{s,t} P^{m}_{s,t} + \rho^{m}_{r,t} P^{m}_{r,t}) \right]^2 + \sum_{d=1}^{D_m} \eta_m |P^{m}_{d,t} - P^{m}_{d,t-1}| \right\} \tag{9}$$

$$\text{s.t.:} \quad \sum_{d=1}^{D_m} (\alpha_{d,t} (P^{m}_{d,t})^2 + \beta_{d,t} P^{m}_{d,t} + \lambda_{d,t}) \le C^{m}_{d,t}. \tag{10}$$

In each MG, the upper and lower boundaries of the adjustable power generators meet constraint (4), and the real and imaginary part of voltage satisfies (5), for $d \in \mathcal{D}_m$, $s \in \mathcal{S}_m$, and $i, j \in \mathcal{B}_m$. In the radical IMG, every MG connects to the main

grid directly, there is no connection in MGs, however, in IMG with a daisy chain or mesh topology, e.g., in daisy-chain IMG, adjacent MGs are connected to each other; and in the mesh IMG, any two MGs can be connected to each other, there are interconnections among the MGs [8]. Thus, it is necessary to consider the power flow among the interconnected MGs. The power-flow constraints on buses interconnecting with neighboring MGs are given by

$$\begin{cases} P^m_{g,i} - \sum_j [e_i(e_jG_{ij} - f_jB_{ij}) + f_i(f_jG_{ij} + e_jB_{ij})] = P^m_{l,i} \\ Q^m_{g,i} - \sum_j [f_i(e_jG_{ij} - f_jB_{ij}) - e_i(f_jG_{ij} + e_jB_{ij})] = Q^m_{l,i} \\ \quad i \in \mathcal{M}_m, j \in \mathcal{M}_m \cup \mathcal{M}_{m'} \quad \forall t. \end{cases} \tag{11}$$

From the above formulation, it can be seen that the voltages in the main grid and the MGs are coupled as in (8). Furthermore, for the interconnected MGs, in addition to coupled nodal voltage in (8), there is also a voltage coupling relationship as in (11). So we next decouple these complex problems for developing distributed solutions in Sections III-A and III-B.

C. Problem Decomposition Based on Time Windows

1) Assumptions on Predictions: In the IMG, renewable resources are used widely, which, however, are weather dependent. Moreover, the load demand is always varying over time. So it can be seen from (6)–(11) that using the forecast information may lead to inaccurate energy scheduling, due to the inevitable forecasting error no matter which forecasting method is used [24]. Therefore, some assumptions on renewable power generation and user load demand should be made before solving the optimization problem. These assumptions on predictions serve as the middle ground between the worse-case and the stochastic perspective [18].

Specifically, the relationship between the actual value and the predicted value of renewable power $P_{r,t}$ and load demand $P_{l,t}$ are established as follows:

$$\begin{cases} P_{l,t} = \hat{P}_{l,t} + \sum_{z=1}^{t} f_l(t-z)e_l(z) \\ P_{r,t} = \hat{P}_{r,t} + \sum_{z=1}^{t} f_r(t-z)e_r(z) \end{cases} \tag{12}$$

where $\hat{P}_{l,t}$ and $\hat{P}_{r,t}$ are the predictions of $P_{l,t}$ and $P_{r,t}$, respectively, made at time $z < t$. The prediction error is $\sum_{z=1}^{t} f(t-z)e(z)$, which is modeled as a weighted linear combination of the previous-step error terms [i.e., $e(z)$]. Here, the error terms are independent and identically distributed (i.i.d.) with mean zero and positive-definite covariance Re; and the weight function $f(\cdot)$ satisfies $f(0) = 1$ and $f(t) = 0$ for $t < 0$. Furthermore, the weight function decays with z, i.e., $f(z) \sim 1/z^{\sigma}$, where σ is the decay exponent. This way, the prediction can be updated with time passes according to (12). This assumption is quite close to the situation in practice.

2) Averaging Fixed Horizon Control Algorithm: In order to reduce the impact of prediction error on power distribution, we focus on the online optimal scheduling. The objectives, which are described in Section II-B, consist of two parts: the first part is in the 2-norm form and the second part is in the 1-norm form. So the IMG optimal scheduling problem is a typical online LASSO problem. In [18], AFHC is applied to solve the problem in an online manner, and the online optimal scheduling can asymptotically converge to the offline optimal solution. In this article, the AFHC is adopted to achieve optimal power scheduling in the IMG. We will derive the conditions for the proposed algorithm to achieve the offline optimal in Section III-C. Actually, AFHC is the algorithm that averages the choices made by fixed horizon control (FHC), and AFHC with prediction window size $w+1$ averages the actions of $w+1$ FHC algorithms. The specific AFHC adopted in this article is given in the following.

The objective in the main grid is similar to that in the MGs. We use AFHC to solve the online LASSO problem, taking the problem of main grid as an example. Let the active power be $P^{\mu}_t = [P^{\mu}_{d,t}, P^{\mu}_{s,t}, P^{\mu}_{e,t}]^T$ and the window size of the AFHC be $w+1$. Every set in each window ι is defined as

$$\Psi_{\iota} = \{i : i \equiv \iota \pmod{(w+1)}\} \cap [-w, T], \quad \iota = 0, 1, \ldots, w.$$

To simplify notation, we define

$$\hat{h}_t(P^{\mu}_t) = \left(P^{\mu}_{l,t} + P^{\mu}_{e,t} - (\rho^{\mu}_{d,t}P^{\mu}_{d,t} + \rho^{\mu}_{s,t}P^{\mu}_{s,t} + \rho^{\mu}_{r,t}P^{\mu}_{r,t})\right)^2$$

so the optimization problem in the ιth window becomes

$$\begin{aligned} \min \quad & \sum_{t=\tau}^{\tau+w} \left(\hat{h}_t\big(P^{\mu}_t\big) + \sum_{d=1}^{D_{\mu}} \eta |P^{\mu}_{d,t} - P^{\mu}_{d,t-1}| \right) \\ \text{s.t.:} \quad & (2)-(5), \ \tau \in \Psi_{\iota}. \end{aligned} \tag{13}$$

Let $\{(P^{(\iota)}_{FHC})^{\mu}\}_{t=z}^{z+w}$ represent the solution to (13), and $(P^{(\iota)}_{FHC,t})^{\mu} = 0$ when $t \le 0$. Then for $w+1$ versions of FHC, AFHC can be obtained by averaging the solutions of $w+1$ FHC algorithms, i.e.,

$$\min \quad P^{\mu}_{AFHC,t} = \frac{1}{w+1} \sum_{\iota=0}^{w} \Big(P^{(\iota)}_{FHC}\Big)^{\mu}. \tag{14}$$

3) Problem Decomposition in the Main Grid and Each MG: Based on the above analysis, the offline optimal problem Prob-I (6) and Prob-II (9) can be decomposed into online energy scheduling problems according to AFHC, i.e., (6) and (9) will be replaced by the process of solving a series of small-scale optimization problems, which can effectively reduce the computational complexity and adapt to the time-varying environment.

Then online energy scheduling for the main grid is

$$\begin{aligned} \min \quad & \sum_{t=\tau}^{\tau+w} \left\{ \left[P^{\mu}_{l,t} + P^{\mu}_{e,t} - \left(\rho^{\mu}_{d,t}P^{\mu}_{d,t} + \rho^{\mu}_{s,t}P^{\mu}_{s,t} + \rho^{\mu}_{r,t}P^{\mu}_{r,t}\right)\right]^2 \right. \\ & \left. + \sum_{d=1}^{D_{\mu}} \eta |P^{\mu}_{d,t} - P^{\mu}_{d,t-1}| \right\} \\ \text{s.t.:} \quad & (3),\ (4),\ (5),\ (7),\ (8) \\ & i \in \mathcal{B}_{\mu}, j \in \mathcal{B}_{\mu} \cup \mathcal{M}_m \quad \forall t. \end{aligned} \tag{15}$$

The online energy scheduling for MG m is

$$\begin{aligned} \min \quad & \sum_{t=\tau}^{\tau+w} \left\{ \left[P^{m}_{l,t} + P^{m}_{e,t} - \left(\rho^{m}_{d,t}P^{m}_{d,t} + \rho^{m}_{s,t}P^{m}_{s,t} + \rho^{m}_{r,t}P^{m}_{r,t}\right)\right]^2 \right. \\ & \left. + \sum_{d=1}^{D_m} \eta_m |P^{m}_{d,t} - P^{m}_{d,t-1}| \right\} \end{aligned} \tag{16}$$

$$\text{s.t.:} \quad (3),\ (4),\ (5),\ (10),\ (11)$$
$$i \in \mathcal{B}_m, j \in \mathcal{M}_m \cup \mathcal{M}_{m'} \quad \forall t \quad \forall m.$$

III. Distributed Online Solutions

Through the analysis of the mathematical model in Section II, it can be seen that the system is coupled by the nodal voltages between the main grid and the MGs, and among the interconnected MGs, as shown in (8) and (11), which poses a great challenge to distributed optimization of energy scheduling. To address this challenge, we propose the HODA based on ADMM to achieve distributed energy management. We will show that our hierarchical online algorithm is asymptotically convergent to the optimal offline solution, and has a sublinear regret and a constant (bounded) competitive ratio, i.e., the online solution is equivalent to the offline solution in expectation. We will derive the conditions for the proposed online algorithm to attain these excellent properties in Section III-C.

A. Decoupling Algorithm

Before implementing the distributed optimization, we first define the auxiliary variables to transform the nonconvex constraints into convex ones [22], i.e.,

$$\begin{cases} \xi_{g,i}P_{g,i} \\ -\sum\limits_j \left[e_i\left(e_jG_{ij}-f_jB_{ij}\right)+f_i\left(f_jG_{ij}+e_jB_{ij}\right)\right]=P_{l,i} \\ \gamma_{g,i}Q_{g,i} \\ -\sum\limits_j \left[f_i\left(e_jG_{ij}-f_jB_{ij}\right)-e_i\left(f_jG_{ij}+e_jB_{ij}\right)\right]=Q_{l,i} \end{cases} \tag{17}$$

where $\xi_{g,i}$ and $\gamma_{g,i}$ are the auxiliary variables, which satisfy $\xi_{g,i}^2=1$ and $\gamma_{g,i}^2=1$. Then, (17) is a convex constraint.

In order to make the main grid and each MG operate independently, it is necessary to decouple the coupled voltage relationship in constraints (8) and (11). If the coupled nodal voltage, such as e_j and f_j, $j \in \mathcal{B}_\mu \cup \mathcal{M}_m$, can be known beforehand, then the energy management in the main grid and the MGs can be optimized independently. Similarly, if the coupled voltages among the interconnected MGs, such as e_j and f_j, $j \in \mathcal{M}_m \cup \mathcal{M}_{m'}$, can be obtained in advance, then the EMS in the MGs can also operate autonomously. Motivated by this idea, the slack variables for the coupled voltages are introduced [16]. Then, the coupled power flow between the main grid and the MGs is transformed. For example, (8) is equivalent to

$$\begin{cases} \xi_{g,i}^{\mu}P_{g,i}^{\mu}-\left(e_i^2+f_i^2\right)G_{ii} \\ -\sum\limits_j \left[e_i\left(e_j^iG_{ij}-f_j^iB_{ij}\right)+f_i\left(f_j^iG_{ij}+e_j^iB_{ij}\right)\right]=P_{l,i}^{\mu} \\ \gamma_{g,i}^{\mu}Q_{g,i}^{\mu}+\left(e_i^2+f_i^2\right)B_{ii} \\ -\sum\limits_j \left[f_i\left(e_j^iG_{ij}-f_j^iB_{ij}\right)-e_i\left(f_j^iG_{ij}+e_j^iB_{ij}\right)\right]=Q_{l,i}^{\mu} \\ i \in \mathcal{B}_\mu, j \in \Pi^{\mu}(i) \quad \forall t \end{cases} \tag{18}$$

$$\begin{cases} \left(\xi_{g,i}^{\mu}\right)^2=1 \\ \left(\gamma_{g,i}^{\mu}\right)^2=1 \end{cases} i \in \mathcal{B}_\mu \quad \forall t \tag{19}$$

where e_j^i and f_j^i are the proposed slack variables, which represent the real and imaginary voltages of j "observed" at node i, respectively; and $\Pi^{\mu}(i)$ is the set of nodes connected to i, but does not include i. So the new relationship between the connected nodes i and j becomes

$$\begin{cases} e_j=e_j^i \\ f_j=f_j^i \end{cases} i \in \mathcal{B}_\mu, j \in \Pi^{\mu}(i) \quad \forall t. \tag{20}$$

Similarly, the coupled nodes in the MGs can be transformed.

The reformulated PROB-I, called PROB-I-R is given by

$$\begin{aligned} & F_\mu \doteq (15) \\ \text{s.t.:} \quad & (4),\ (5),\ (7),\ (18)-(20) \\ & i \in \mathcal{B}_\mu, j \in \Pi^{\mu}(i) \quad \forall t \end{aligned} \tag{21}$$

where F_μ is the main grid cost in one window. The reformulated PROB-II$_m$, called PROB-II-R$_m$, is given by

$$F_m \doteq (16) \tag{22}$$
$$\text{s.t.:} \quad (4),(5),\ (10) \tag{23}$$
$$\xi_{g,i}^{m}P_{g,i}^{m}-\left(e_i^2+f_i^2\right)G_{ii}- \sum_{j\in\Pi^m(i)}\left[e_i\left(e_j^iG_{ij}-f_j^iB_{ij}\right)+f_i\left(f_j^iG_{ij}+e_j^iB_{ij}\right)\right]=P_{l,i}^{m} \tag{24}$$
$$\gamma_{g,i}^{m}Q_{g,i}^{m}+\left(e_i^2+f_i^2\right)B_{ii}- \sum_{j\in\Pi^m(i)}\left[f_i\left(e_j^iG_{ij}-f_j^iB_{ij}\right)-e_i\left(f_j^iG_{ij}+e_j^iB_{ij}\right)\right]=Q_{l,i}^{m} \tag{25}$$
$$\left(\xi_{g,i}^{m}\right)^2=1 \tag{26}$$
$$\left(\gamma_{g,i}^{m}\right)^2=1 \tag{27}$$
$$e_j=e_j^i \tag{28}$$
$$f_j=f_j^i \tag{29}$$
$$i \in \mathcal{B}_m, j \in \Pi^m(i) \quad \forall t \quad \forall m.$$

For the coupled main grid and the MGs, we have $\Pi^m(i) \subset \mathcal{B}_\mu$. For the interconnected MGs, there is another coupling voltage constraint for MG m and MG M'. Specifically, for MG m, we have $\Pi^m(i) \subset (\mathcal{B}_\mu \cup \mathcal{B}_{m'})$.

This way, the problems in the main grid and MGs become optimal problems with equality coupling relationship, i.e., (20), (28), and (29). In each EMS, this coupled constraint can be tackled more easily as explained in the remainder of this section. Thus, the main grid and the MGs can operate in an autonomous and distributed manner. The specific method to achieve this goal will be discussed in Section III-B.

B. Hierarchical Algorithm Based on ADMM

According to the above discussions, it can be seen that the optimal energy scheduling problems in the main grid and MGs are both *online LASSO* problems with linear coupled equality constraints, and the objective functions in the IMG are decomposable as discussed in Section II. This mathematical problem can be solved well using the ADMM algorithm.

As discussed in Section II-B, there is 1-norm in the objective functions. So before presenting the proposed algorithm, we first adopt a soft-thresholding operator to rewrite the nondifferentiable objective function. In one rolling window,

the objective functions in (15) and (16) can be written, respectively, as

$$\begin{aligned} \min \quad & \|P^{\mu}_{\text{net}} - H^{\mu}P^{\mu}_{M}\|_2^2 + \eta^{\mu}\|U^{\mu}P^{\mu}_{sub}\|_1 \qquad (30)\\ \min \quad & \|P^{m}_{\text{net}} - H^{m}P^{m}_{MG}\|_2^2 + \eta^{m}\|U^{m}P^{m}_{sub}\|_1 \qquad (31)\\ & m = 1, 2, \ldots, M \end{aligned}$$

where

$$\begin{aligned} P^{\mu}_{\text{net}} &= \left[\left(P^{\mu}_{l,\tau} - \rho^{\mu}_{r,\tau}P^{\mu}_{r,\tau}\right), \ldots, \left(P^{\mu}_{l,\tau+w} - \rho^{\mu}_{r,\tau+w}P^{\mu}_{r,\tau+w}\right)\right]^T\\ P^{\mu}_{M} &= \left[\left(P^{\mu}_{d,\tau}, P^{\mu}_{s,\tau}, P^{\mu}_{e,\tau}\right), \ldots, \left(P^{\mu}_{d,\tau+w}, P^{\mu}_{s,\tau+w}, P^{\mu}_{e,\tau+w}\right)\right]^T \end{aligned}$$

and $P^{\mu}_{M,\tau}$ denotes the controllable generator in the main grid at time τ. Here, the elastic load is treated as a negative generator, i.e.,

$$\begin{aligned} H^{\mu} = \ & \Big[\left(\rho^{\mu}_{d,\tau}, \rho^{\mu}_{s,\tau}, -1, 0, \ldots, 0\right); \cdots;\\ & \left(0, \ldots, 0, \rho^{\mu}_{d,\tau+w}, \rho^{\mu}_{s,\tau+w}, -1\right)\Big]^T\\ U^{\mu}P^{\mu}_{sub} = \ & \Big[\left(x_{\mu,\tau}, x_{\mu,\tau+1}, \ldots, x_{\mu,\tau+w}\right)^T\\ & - \left(x_{\mu,\tau-1}, x_{\mu,\tau}, 0, 0, \ldots, 0\right)^T\Big]. \end{aligned}$$

Correspondingly, P^{m}_{net}, x^m, H^m, and $U^m u^m$ in MG m can be obtained in the same way. Then, the method in [19] is used to solve this problem.

According to the analysis in Section III-A, we first formulate the augmented Lagrangian of PROB-I-R to decouple the constraints in the main grid and MGs, given by

$$\begin{aligned} & L_{\delta^{\mu}}\left(x^{\mu}, u^{\mu}, z^{\mu}, \varphi^{\mu}\right)\\ & = \|P^{\mu}_{\text{net}} - H^{\mu}P^{\mu}_{M}\|_2^2 + \eta^{\mu}\|U^{\mu}P^{\mu}_{sub}\|_1\\ & \quad + \sum_{i\in\mathcal{B}_{\mu}}\sum_{j\in\Pi^{\mu}(i)}\left[\left(\zeta^{j}_{i}\right)^{\mu}\left(e_i - e^{j}_{i}\right) + \left(\psi^{j}_{i}\right)^{\mu}\left(f_i - f^{j}_{i}\right)\right]\\ & \quad + \frac{\delta^{\mu}}{2}\sum_{i\in\mathcal{B}_{\mu}}\sum_{j\in\Pi^{\mu}(i)}\left[\left(e_i - e^{j}_{i}\right)^2 + \left(f_i - f^{j}_{i}\right)^2\right] \qquad (32)\\ & \text{s.t.:} \quad (4), (5), (7), (18), (19)\\ & \quad i \in \mathcal{B}_{\mu}, j \in \Pi^{\mu}(i) \quad \forall t \end{aligned}$$

where ζ^{μ} and ψ^{μ} are the dual variables; $\delta^{\mu} > 0$ is the augmented Lagrangian parameter; $x^{\mu} = [P^{\mu}_{M,t}, Q^{\mu}_{t}, e_i, f_i, \xi^{\mu}_{g,i}, \gamma^{\mu}_{g,i}]$; $Q^{\mu}_{t} = [Q^{\mu}_{d,t}, Q^{\mu}_{s,t}Q^{\mu}_{e,t}, Q^{\mu}_{r,t}]$; $u^{\mu} = P^{\mu}_{sub}$, and $z^{\mu} = [e^{i}_{j}, f^{i}_{j}]$, for all $j \in \Pi^{\mu}(i)$; $\zeta^{\mu} = \{(\zeta^{i}_{j})^{\mu}\}$; $\psi^{\mu} = \{(\psi^{i}_{j})^{\mu}\}$, $i \in \mathcal{B}_{\mu}, j \in \Pi^{\mu}(i)$; and $\varphi^{\mu} = [\zeta^{\mu}, \psi^{\mu}]$.

The augmented Lagrangian of PROB-II-R$_m$ is given by

$$\begin{aligned} & L_{\delta^{m}}\left(x^{m}, z^{m}, \varphi^{m}\right)\\ & = \|P^{m}_{\text{net}} - H^{m}P^{m}_{MG}\|_2^2 + \eta^{m}\|U^{m}P^{m}_{sub}\|_1\\ & \quad + \sum_{i\in\mathcal{B}_{\mu}}\sum_{j\in\mathcal{B}_{m}}\left[\left(\zeta^{j}_{i}\right)^{m}\left(e_i - e^{j}_{i}\right) + \left(\psi^{j}_{i}\right)^{m}\left(f_i - f^{j}_{i}\right)\right]\\ & \quad + \frac{\delta^{\mu}}{2}\sum_{i\in\mathcal{B}_{\mu}}\sum_{j\in\mathcal{B}_{m}}\left[\left(e_i - e^{j}_{i}\right)^2 + \left(f_i - f^{j}_{i}\right)^2\right]\Bigg\} \qquad (33)\\ & \text{s.t.:} \quad (23)-(27) \quad \forall t \quad \forall m. \end{aligned}$$

Problems (32) and (33) can be solved iteratively by ADMM for the radial IMG as follows:

$$\begin{cases} (x^{\mu})^{(k+1)} := \arg\min L_{\delta^{\mu}}\left(x^{\mu}, (u^{\mu})^{k}, (z^{\mu})^{k}, (\varphi^{\mu})^{k}\right)\\ (x^{m})^{(k+1)} := \arg\min L_{\delta^{m}}\left(x^{m}, (u^{m})^{k}(z^{m})^{k}, (\varphi^{m})^{k}\right) \end{cases} \qquad (34)$$

where $x^{\mu} \in \chi^{\mu}$, χ^{μ} is the set which is composed of constraints (4), (5), (7), and (18); $x^{m} \in \chi^{m}$; $x^{m} = [P^{m}_{g,i}, P^{m}_{s,i}, P^{m}_{e,i}, Q^{m}_{g,i}, Q^{m}_{s,i}, Q^{m}_{e,i}, Q^{m}_{r,i}, e_i, f_i, \xi^{m}_{g,i}, \gamma^{m}_{g,i}]$; $i \in \mathcal{B}_m$, for all t; and χ^{m} is composed by (23)–(27)

$$\begin{cases} (u^{\mu})^{(k+1)} := S_{(\eta^{\mu},\zeta^{\mu},\psi^{\mu})}\left((x^{\mu})^{(k+1)}, u^{\mu}, (z^{\mu})^{k}, (\varphi^{\mu})^{k}\right)\\ (u^{m})^{(k+1)} := S_{(\eta^{m},\zeta^{m},\psi^{m})}\left((x^{m})^{(k+1)}, u^{m}, (z^{m})^{k}, (\varphi^{m})^{k}\right) \end{cases} \qquad (35)$$

here u^{μ} and u^{m} are in the 1-norm term, and $S_{(\eta^{\mu},\zeta^{\mu},\psi^{\mu})}$ and $S_{(\eta^{m},\zeta^{m},\psi^{m})}$ are the soft-thresholding operators, as discussed in [19, Sec. 4.4.3]

$$\begin{cases} (z^{\mu})^{(k+1)} := \arg\min L_{\delta^{\mu}}\left((x^{\mu})^{(k+1)}, (u^{\mu})^{(k+1)}, z^{\mu}, (\varphi^{\mu})^{k}\right)\\ (z^{m})^{(k+1)} := \arg\min L_{\delta^{m}}\left((x^{m})^{(k+1)}, (u^{m})^{(k+1)}\right.\\ \left. z^{m}, (\varphi^{m})^{k}\right) \end{cases} \qquad (36)$$

where $z^{\mu} \in \phi^{\mu}$; ϕ^{μ} is the set satisfying (18); $z^{m} \in \phi^{m}$, and (28) and (29) consist of ϕ^{m}, $j \in \Pi^{m}(i) \subset \mathcal{B}_{\mu}$.

In order to simplify the linear equation constraints (20), (28), and (29), we rewrite the relationship as $A^{\mu}(x^{\mu}) + B^{\mu}(z^{\mu}) = 0$ in the main grid, and $A^{m}(x^{m}) + B^{m}(z^{m}) = 0$ in MG m. Then, the dual variables are updated as follows:

$$\begin{cases} (\varphi^{\mu})^{(k+1)} := (\varphi^{\mu})^{k} + \delta^{\mu}\left(A^{\mu}(x^{\mu})^{(k+1)} + B^{\mu}(z^{\mu})^{(k+1)}\right)\\ (\varphi^{m})^{(k+1)} := (\varphi^{m})^{k} + \delta^{m}\left(A^{m}(x^{m})^{(k+1)} + B^{m}(z^{m})^{(k+1)}\right). \end{cases} \qquad (37)$$

For interconnected MGs, the coupled constraints (28) and (29) are not only related to the main grid but also to all the MG m's that are connected to MG m. If the MG is only connected to adjacent MGs, we have $m' \in \{m-1, m+1\}$. If MG m is connected to any other MGs, then the set is different, i.e., $m' \in \{1, 2, \ldots, M | m' \neq m\}$. Correspondingly, the z^m and φ^m in (36) and (37) will take different forms for IMG with a different connection structure.

This way, (34)–(36) can be solved independently in the M-EMS and MG-EMS, (37) can be solved in the DNO at the top layer to obtain the updated dual variables. Then, the DNO sends them to the M-EMS and MG-EMS in the second layer to optimize the power scheduling. It can be seen that whether the MG is connected to the main grid or connected to other MGs, the proposed HODA scheme can be used to decouple the problem and optimize its energy distribution, so each MG and the main grid can both achieve autonomous energy management.

C. Online Optimization Indicator and Conditions

To ensure convergence for the online algorithm solution, i.e., asymptotically to the offline optimal solution, the AFHC method is employed to solve the hierarchical scheduling

problem. In order to evaluate the performance of the online algorithm, here we define the online optimization as

$$C_{\text{on}} = (34)-(37) \quad \forall t \tag{38}$$

where C_{on} denotes the online cost result. Correspondingly, the static offline optimization is defined as

$$\begin{aligned} &C_{\text{off}} = (1) \\ &\text{s.t.} \quad (2)-(5) \quad \forall t \end{aligned} \tag{39}$$

where C_{off} is the offline optimization cost.

For the AHFC-based online optimization algorithm, if the predicted renewable output power $\hat{P}_{r,t}$ and load demand $\hat{P}_{l,t}$ satisfy assumption (12) in Section II-C and the predicted net power $\hat{P}_{\text{net},t}$ satisfies condition (40), we have

$$\begin{aligned} &\inf_{\hat{P}_{\text{net},t}} \left\{ \mathbb{E}_e \left\{ \sum_{t=1}^{T} \sum_{u=1}^{U} \left(AA^{\dagger} \left(P_{\text{net},t} - \frac{1}{T} \sum_{t=1}^{T} P_{\text{net},t} \right) \right)^2 \right\} \right\} \\ &\geq \varepsilon T \end{aligned} \tag{40}$$

where $A = [\rho_{d,t}, \rho_{s,t}, -1]^T$; $A^{\dagger}$ is the Moore–Penrose pseudoinverse of A; ε is a constant when w, Re, η, and A are known; and $\varepsilon = f(Re, w)$. According to [18], AFHC is strictly convergent, and it can achieve a sublinear regret and constant competitive ratio, i.e., the following formulations hold true:

$$\sup_{\hat{P}_{l,t}, \hat{P}_{r,t}} \{\mathbb{E}_e[C_{\text{on}} - C_{\text{off}}]\} \leq \phi(T) \tag{41}$$

$$\sup_{\hat{P}_{l,t}, \hat{P}_{r,t}} \frac{\mathbb{E}_e[C_{\text{on}}]}{\mathbb{E}_e[C_{\text{off}}]} \leq \upsilon(T) \tag{42}$$

where $\phi(T)$ will be 0 and $\upsilon(T)$ will be a constant.

D. Hierarchical Online Distributed Algorithms

In this section, we summarize the analysis in the previous sections and present the proposed HODA scheme for the entire IMG system. As discussed, HODA consists of two layers: 1) the top layer mainly on the exchange and update of dual variables to ensure the convergence of ADMM and 2) the lower layer focusing on distributed online energy distribution in the main grid and the MGs independently. The proposed scheme is presented in Algorithms 1 and 2.

The proposed HODA leverages ADMM to decouple the coupled constraints in the main grid and MGs, and ADMM is also employed to deal with the 1-norm term in the objective functions. According to [19, Sec. 3.2], ADMM ensures the convergence of the two-layer decomposition. Therefore, HODA is a convergent, distributed algorithm for IMG.

Furthermore, in Section III-C, we discuss the condition of convergence for the online optimization and show the bounds on the gap and ratio of the online and offline results in (41) and (42). If the error of prediction is independent (i.e., the error is i.i.d. noise), the sliding window of size w can be the entire time horizon T; otherwise, it is less than T and a finite constant according to [18, Th. 5 and Corollary 6]. Thus, in (41), the time-average loss of the online algorithm goes to zero as T goes to infinity, when it satisfies the above conditions. In (42), the algorithm's competitive ratio (bound) goes to 1 in expectation. This means the HODA algorithm solution for online energy scheduling in the IMG converges asymptotically to the offline optimal solution.

Finally, we examine the complexity of the proposed algorithms. Problem (34) is a nonlinear convex problem, which

Algorithm 1: Top Layer Algorithm

Step 1: Initialization: set window size w, MG number M, time period T, the maximum number of iterations K, all 'observed' voltages $\{e_j^i, f_j^i\}$ that are coupled in the IMG, the dual variables $\{\varphi^{\mu}, \varphi^m\}$, and the augmented Lagrangian parameter $\{\delta^{\mu}, \delta^m\}$;
Step 2: Send the updated dual variables $\{(\varphi^{\mu})^k, (\varphi^m)^k\}$ to the M-EMS and each MG EMS in the lower layer to execute Algorithm 2;
Step 3: Receive $\{(x^{\mu})^{(k+1)}, (x^m)^{(k+1)}, (u^{\mu})^{(k+1)}, (u^m)^{(k+1)}, (z^{\mu})^{(k+1)}, (z^m)^{(k+1)}\}$ from the M-EMS and each MG EMS, respectively, and then update dual variables $\{(\varphi^{\mu})^{(k+1)}, (\varphi^m)^{(k+1)}\}$ according to (37);
Step 4: Check whether ADMM satisfies its convergence criteria [19]. If yes, send the updated dual variables to Step 5 of Algorithm 2 for obtaining the optimal values $(x^{\mu})^*$ and $(x^m)^*$; Otherwise, $k := k+1$. If $k \leq K$, jump to Step 2; Otherwise, exit.

Algorithm 2: Lower Layer Algorithm

Step 1: $\Psi_{\iota} = \{i : i \equiv \iota \pmod{(w+1)}\} \cap [-w, T]$, $\iota = 0, 1, \ldots, w$, and set $t = 1$ and $\iota = 0$;
Step 2: For $\tau \in \Psi_m$, and then for $t = \tau, \tau+1, \ldots, \tau+w$, update the renewable power and load demand in the Main Grid and MGs as in (12), defined as $\{P_{r,t}\}_{t=\tau}^{\tau+w}$ and $\{P_{l,t}\}_{t=\tau}^{\tau+w}$;
Step 3: Receive $(\varphi^{\mu})^k$ and $(\varphi^m)^k$ from Algorithm 1, and solve the power energy distribution problem given in (34)–(36) in the Main Grid and each MG independently;
Step 4: Send the updated dual variables $(x^{\mu})^{(k+1)}$, $(x^m)^{(k+1)}$, $(u^{\mu})^{(k+1)}$, $(u^m)^{(k+1)}$, $(z^{\mu})^{(k+1)}$, and $(z^m)^{(k+1)}$ to the top layer for updating the dual variables;
Step 5: Receive the converged dual variables from Step 4 of Algorithm 1, and optimize (34) in the Main Grid and MG EMSs independently;
Step 6: Obtain solution $\{(P_{FHC,t}^{(\iota)})^{\mu}\}_{t=\tau}^{\tau+w}$ in the Main Grid and $\{(P_{FHC,t}^{(\iota)})^m\}_{t=\tau}^{\tau+w}$ in MG m, and compute

$$P_{AFHC,t}^{\mu} = \frac{1}{w+1} \sum_{\iota=0}^{w} \left(P_{FHC,t}^{(\iota)} \right)^{\mu} \tag{43}$$

$$P_{AFHC,t}^{m} = \frac{1}{w+1} \sum_{\iota=0}^{w} \left(P_{FHC,t}^{(\iota)} \right)^{m}; \tag{44}$$

Step 7: Set $\iota = \iota + 1$ and $t = t + 1$;
Step 8: If $\iota \geq w$, reset $\iota = 0$. If $t \leq T$, reset $k = 0$, send k to Step 2 of Algorithm 1, and go to Step 2 of Algorithm 1; Otherwise, exit.

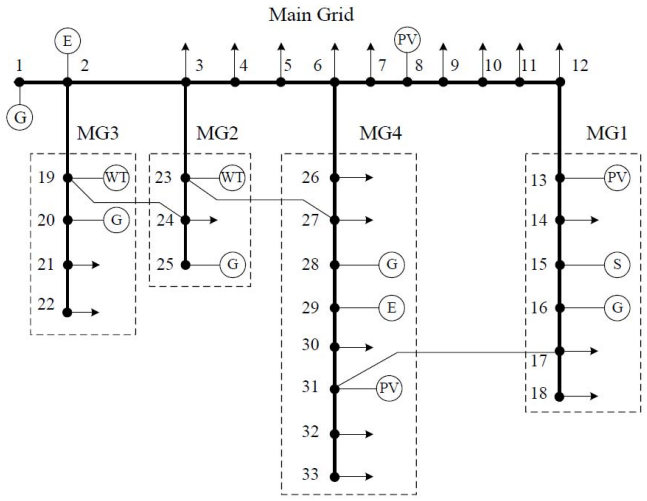

Fig. 2. Configuration of the real-world IMG system deployed in the Hekou town, Nantong City, Jiangsu Province, China.

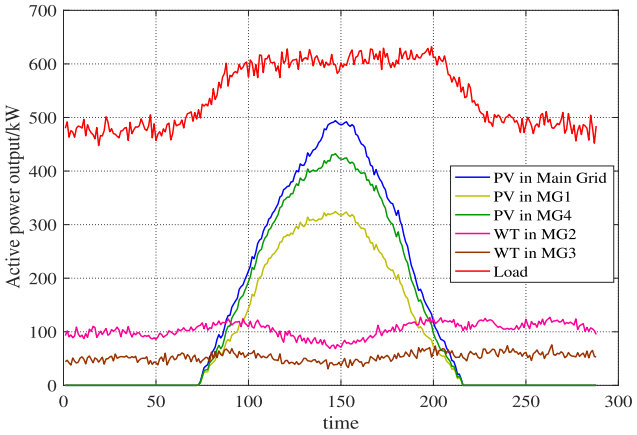

Fig. 3. Renewable power and load demand profiles of the IMG shown in Fig. 2.

TABLE III
NUMBER OF VARIABLES, CUP TIME IN HODA AND OEM

Algorithm	Number of Variables	CPU time (s)
HODA	106	1.85
OEM	246	151.32

can be solved with the Davidon–Fletcher–Powell (DFP) algorithm. The complexity of DFP is $\mathcal{O}(n^2)$ according to [25]. Problem (35) is solved by the soft-thresholding operator directly, with a constant time complexity. Finally, problem (36) is a linear programming (LP) problem, which can be solved by an LP solver with complexity $\mathcal{O}(n\log(n))$ [26]. According to Algorithm 1, there will be at most k iterations. Combining Algorithms 1 and 2, we can see that the time complexity of the entire algorithm is $k(\mathcal{O}(n^2) + \mathcal{O}(n\log(n)))$, for $k < K$, where K is a constant in computation. So the time complexity of the proposed HODA is $\mathcal{O}(n^2)$.

IV. Simulation Study

The performance of the proposed HODA is evaluated in this section by applying it to a real IMG system. We first present the specific parameter settings and configuration of the real IMG system in Section IV-A. The performance of the optimal online distributed scheduling for IMG with different topologies is presented in Section IV-B. Finally, Section IV-C examines the convergence performance of HODA.

A. Configuration and Parameter Setting of the Real-World IMG System

For performance evaluation, we consider a real-world IMG system deployed in the Hekou town, Nantong City, Jiangsu Province, China (the GPS coordinates are 32.49°N and 120.83°E). The IMG system consists of the main grid and four MGs, each having PVs, WTs, diesel generators, battery ESS, fixed load demands, and elastic loads, as shown in Fig. 2. The IMG has a typical link topology according to the method in [15] and [27]. It is an IEEE-33-based power system. For the link connection structure, each MG connects to the main grid, and there is also an electrical connection between these MGs, as shown in Fig. 1. In Section IV-B, we also test the proposed algorithms with an IMG with a mesh topology, which is constructed by adding a connection between nodes {22, 33} in Fig. 2.

The renewable power profiles in the main grid and each MG are shown in Fig. 3. We consider both PV or WT in each MG and the main grid. We also consider both fixed and elastic loads in the system. Fig. 3 shows the fixed load demand, which is mainly from the factory in town. The elastic load is mainly from the air conditioners and pumping systems.

For online optimization of power scheduling, the operation can be performed every 2 h, 1 h, 0.5 h, or 15 min. The actual timescale of operation is varied according to users' power demand. In this article, the parameter for HODA is set to 30 min, as one window size. For the proposed online algorithm, during simulation, we run the proposed online algorithm for one day, and set the time interval in the model to 5 min. Therefore, there are $T = 288$ time intervals in total.

All the simulations are executed in MATLAB to verify the proposed HODA performance. HODA only takes no more than 2 s to solve the optimal energy scheduling problem in the main grid or each MG. We compare the number of variables and CUP time of HODA and the online energy management (OEM) scheme in [4], as shown in Table III. There are in total 106 variables in HODA, and the most variables in M-EMS are 32. So the autonomous energy management in IMG executes much faster. HODA is more suitable for online optimization and real-time control of the power system.

B. Performance Evaluation

In order to testify the performance of the proposed HODA, it is applied to the linked IMG as shown in Fig. 2. In the IMG, controllable power includes diesel generator's output and battery charging/discharging power in the main grid and every MG. The elastic load comes from the main grid and MG 4 as shown in Fig. 2. The battery is in MG 1. Fig. 4 presents the overall scheduling results of the IMG system, while Fig. 5

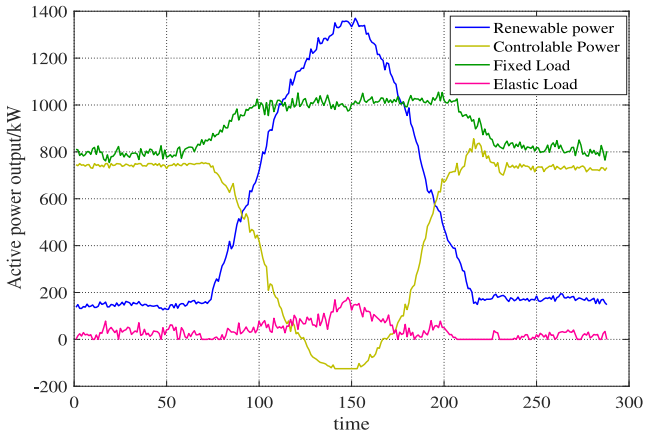

Fig. 4. Renewable, controllable power, and load demand in the link IMG achieved by HODA.

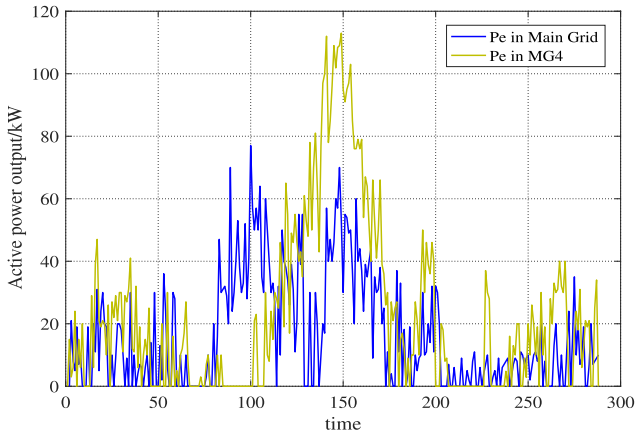

Fig. 6. Elastic load in the link IMG achieved by HODA.

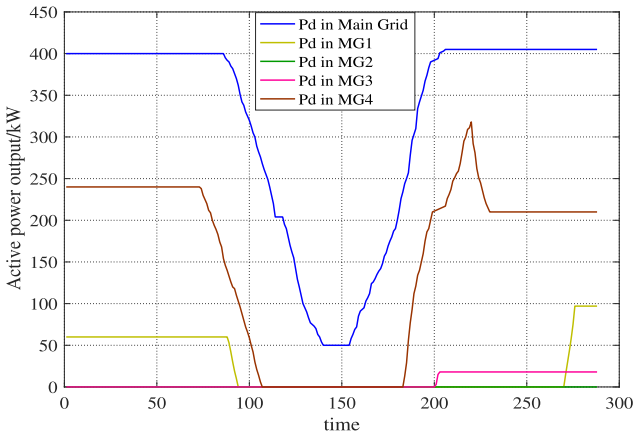

Fig. 5. Diesel generator's power output in the link IMG achieved by HODA.

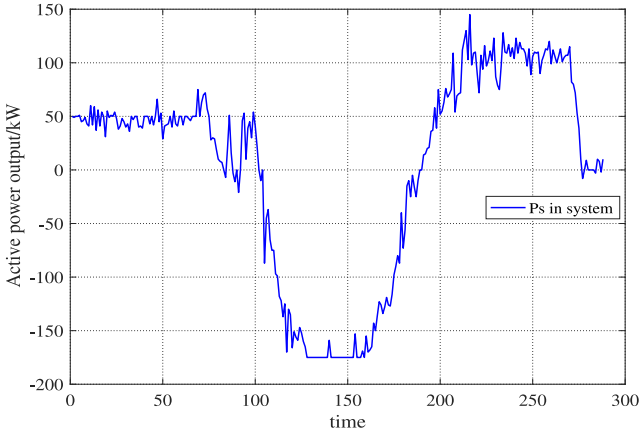

Fig. 7. Charge/discharge power of the batteries in the link IMG achieved by HODA.

shows the distributed optimization on the diesel generator's output power. In the beginning of Fig. 4, the diesel generator, battery, and WT provide power to satisfy the load demand, and the elastic load is used to absorb the surplus energy to guarantee a smooth output power from the diesel generator, as shown in Fig. 5.

During mid-noon, from $t = 112$ to $t = 178$, renewable power becomes obviously larger than the load demand (e.g., due to higher solar intensity), as shown in Fig. 4. The EMS in MG 1 regulates the batteries to start charging, and the EMS in the main grid and MG 4 control their elastic load to absorb the excess energy, as shown in Figs. 6 and 7.

With the proposed HODA, the main grid and each MG can have autonomous energy management and achieve optimal energy scheduling. As shown in Fig. 5, the output of the diesel generators is highly stable in the main grid and every MG.

From Fig. 5, it can be seen that P_d in the main grid, MG 1, and MG 4 start to decrease gradually from time $t = 72$ to $t = 108$, since the PV power generation increases gradually during this period. The diesel generator's output powers in MG 1 and MG 4 become both 0 when the PV power is sufficient for satisfying the load from $t = 95$ to $t = 184$. When the PV power generation begins to decrease, P_d in the main grid and MG 4 starts to increase. While the diesel generator in MG 1 is restarted when $t = 272$, because the batteries stop to discharge. Furthermore, when the load demand is larger than the diesel and PV power generation in MG4, the batteries in MG 1 offer energy to ensure that P_d increases smoothly, as the brown line in Fig. 5 shows. P_d in MG 2 is always 0 for renewable energy generated in this MG can always meet the load demand, and the excess energy is mainly sold to MG 4. P_d in MG 3 is 0 from $t = 1$ to $t = 202$, since the WT power is sufficient. When the WT power is not able to meet the load demand, the diesel generator in MG 3 is started to increase power generation smoothly. Since in the IMG, the diesel generator in the main grid is the slack generator, and the load demand in the main grid is larger than the MGs, the diesel generator in the main grid is always on and provides the reference voltage for the system, as shown in Fig. 5.

In addition to enabling autonomous energy management in *linked* IMG, we also apply the proposed HODA scheme to IMG with the *radial* and *mesh* topologies. The diesel generators' power outputs achieved by HODA for the three IMG are shown in Fig. 8. It can be seen that the total diesel generators' power is less in the IMG with a mesh topology; because of the electrical connection between the MGs, the MGs with a mesh

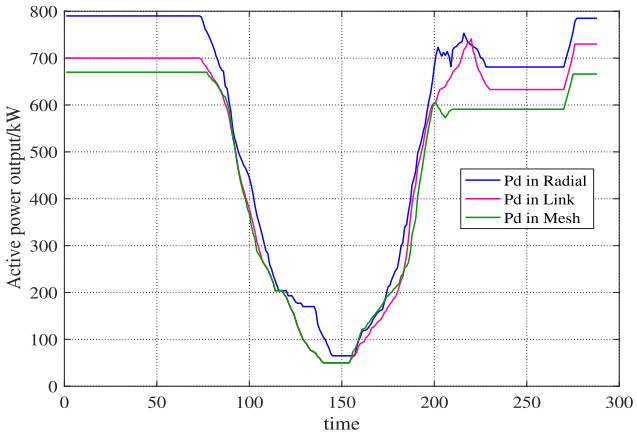

Fig. 8. Diesels power generation in three IMG with different topologies as achieved by HODA.

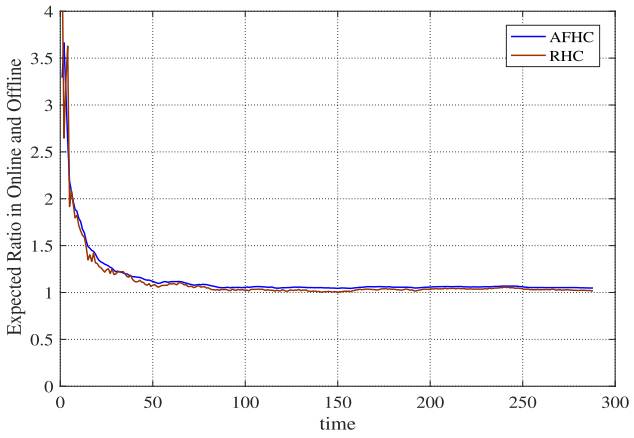

Fig. 9. Expected competitive ratios achieved by the two online algorithms (AFHC and RHC) in online and offline cases.

topology can make better use of the renewable energy. When the WT power is larger than the load in MG 2 and MG 3 at the beginning, these two MGs can sell the surplus energy to MG 4 and MG 1. Consequently, the P_d's in MG 4 and MG 1 are less than that in the radial and link IMG, respectively. It can also be seen that the P_d power is the largest in the radial IMG, for there is only energy purchase allowed from the main grid, but no energy trading can be done among the MGs. Thus, the renewable resources are not fully utilized.

The above simulation results clearly show that the proposed HODA scheme has the excellent distributed energy management performance for IMG with any topologies. Furthermore, the figures show excellent performance on maximizing the users' satisfaction and utilization of renewable resources. Figs. 5 and 8 demonstrate the effectiveness of the proposed scheme for minimizing the variation in the output power of diesel generators in every system.

C. Convergence of HODA

In order to verify the convergence performance of the proposed HODA, we compare our online algorithm with the rolling horizon control (RHC) method, which is very popular in online scheduling in the smart grid and MGs [28], [29]. First, we formulate the optimal offline problem that minimizes the objective function C_{off} over the entire time horizon T. Then the same online energy scheduling problem is solved by AFHC and RHC, respectively, and the results are plotted in Figs. 9 and 10. As in (42), we find that the online solutions solved by AFHC and RHC are both convergent. The online scheduling competitive ratio traces (as compared to the offline optimal solution) are shown in Fig. 9. It is obvious that the competitive ratio is

$$\lim_{T\to\infty} \upsilon(T) \to 1. \tag{45}$$

This means that the results solved by AFHC and RHC both converge to the offline optimal solution if the time is sufficiently long.

Fig. 10 shows the expected difference between the online results solved by AFHC and FHC and the offline optimal result

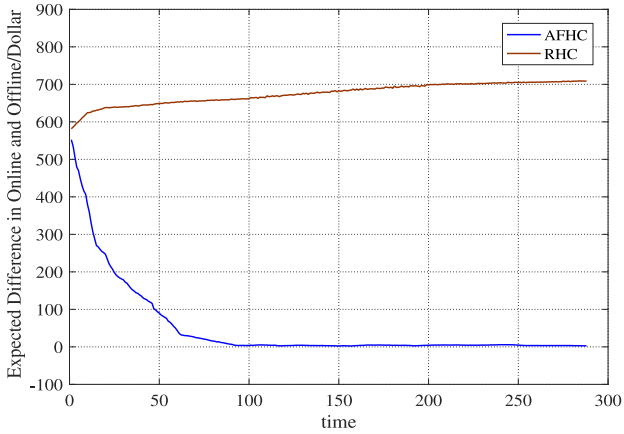

Fig. 10. Expected regret in online and offline cases.

(i.e., the optimality gap). The simulation results show that the expectation of the AFHC optimality gap is

$$\lim_{T\to\infty} \phi(T) \to 0. \tag{46}$$

This is mainly due to the assumption on our prediction model in (12), which can capture the important features of real predictors. And the online problem (14) averages the solutions of $(w+1)$ FHC algorithms, so the error in prediction is offset in the calculation. When (13) is solved by RHC, the errors in prediction are not mitigated, and the error gradually accumulates over time, resulting in an increasingly optimality larger gap, as the brown line in Fig. 10 shows.

From Figs. 9 and 10, the outstanding convergence performance of the proposed HODA scheme is primarily due to the assumption on our prediction model in (12), which can capture the essential features of real predictors. Furthermore, when we attempt to look ahead further into the future, the quality of prediction will become lower, which is closer to the actual forecasting. As described in (14), the online optimal results not only take into account future predictions but also effectively use the historical values, which bring them closer to the offline optimal value. Furthermore, in our model,

predictions are refined over time and they are sufficiently flexible to mitigate the forecast error on time series.

V. Conclusion

In this article, an optimal online algorithm, called HODA, was proposed to solve the power distribution and decoupling problems in the IMG. Our problem formulation both maximized users' satisfaction and minimized the variation in diesel generator generation. The formulated problem was an online LASSO problem with coupled constraints. In order to achieve distributed energy management, ADMM was introduced to decouple this complexity problem and achieve hierarchical energy optimization. To verify the effectiveness of HODA, we applied it to a real-world IMG. The results showed that HODA could effectively decouple and optimize the power scheduling in IMG. Furthermore, we showed that HODA asymptotically converged to the offline optimal solution. In addition, the proposed HODA algorithm could effectively achieve the goals of smoothing the output of diesel power generation and optimizing the distribution of energy.

Acknowledgment

The authors would like to thank Prof. X. Liu with the Chinese Academy of Sciences for his help on solving the nonsmooth convex problems with ADMM.

References

[1] X. Wang, X. Wang, and S. Mao, "RF sensing for Internet of Things: A general deep learning framework," *IEEE Commun. Mag.*, vol. 56, no. 9, pp. 62–67, Sep. 2018.

[2] J. Lin, W. Yu, N. Zhang, X. Yang, H. Zhang, and W. Zhao, "A survey on Internet of Things: Architecture, enabling technologies, security and privacy, and applications," *IEEE Internet Things J.*, vol. 4, no. 5, pp. 1125–1142, Oct. 2017.

[3] Y. Wang, S. Mao, and R. M. Nelms, "On hierarchical power scheduling for the macrogrid and cooperative microgrids," *IEEE Trans. Ind. Informat.*, vol. 11, no. 6, pp. 1574–1584, Dec. 2015.

[4] H. Zou, Y. Wang, S. Mao, F. Zhang, and X. Chen, "Online energy management in microgids considering reactive power," *IEEE Internet Things J.*, vol. 6, no. 2, pp. 2895–2906, Apr. 2019.

[5] M. J. Hossain, M. A. Mahmud, F. Milano, S. Bacha, and A. Hably, "Design of robust distributed control for interconnected microgrids," *IEEE Trans. Smart Grid*, vol. 7, no. 6, pp. 2724–2735, Nov. 2016.

[6] K. Utkarsh, D. Srinivasan, A. Trivedi, W. Zhang, and T. Reindl, "Distributed model-predictive real-time optimal operation of a network of smart microgrids," *IEEE Trans. Smart Grid*, vol. 10, no. 3, pp. 2833–2845, May 2019.

[7] L. Che, X. Zhang, M. Shahidehpour, A. Alabdulwahab, and A. Abusorrah, "Optimal interconnection planning of community microgrids with renewable energy sources," *IEEE Trans. Smart Grid*, vol. 8, no. 3, pp. 1054–1063, Nov. 2017.

[8] H. Zou, S. Mao, Y. Wang, F. Zhang, X. Chen, and L. Cheng, "A survey of energy management in interconnected multi-microgrids," *IEEE Access*, vol. 7, pp. 72158–72169, 2019.

[9] J. Lee, J. Guo, J. K. Choi, and M. Zukerman, "Distributed energy trading in microgrids: A game-theoretic model and its equilibrium analysis," *IEEE Trans. Ind. Electron.*, vol. 62, no. 6, pp. 3524–3533, Jun. 2015.

[10] H. Wang and J. Huang, "Incentivizing energy trading for interconnected microgrids," *IEEE Trans. Smart Grid*, vol. 9, no. 4, pp. 2647–2657, Jul. 2018.

[11] A. M. Jadhav, N. R. Patne, and J. M. Guerrero, "A novel approach to neighborhood fair energy trading in a distribution network of multiple microgrid clusters," *IEEE Trans. Ind. Electron.*, vol. 66, no. 2, pp. 1520–1531, Feb. 2019.

[12] K. Rahbar, C. C. Chai, and R. Zhang, "Energy cooperation optimization in microgrids with renewable energy integration," *IEEE Trans. Smart Grid*, vol. 9, no. 2, pp. 1482–1493, Mar. 2018.

[13] K. Rahbar, C. C. Chai, and R. Zhang, "Real-time energy management for cooperative microgrids with renewable energy integration," in *Proc. IEEE Int. Conf. Smart Grid Commun. (SmartGridComm)*, Venice, Italy, Nov. 2014, pp. 25–30.

[14] H. Abdi, S. D. Beigvand, and M. L. Scala, "A review of optimal power flow studies applied to smart grids and microgrids," *Renew. Sustain. Energy Rev.*, vol. 71, pp. 742–766, May 2017.

[15] W.-J. Ma, J. Wang, V. Gupta, and C. Chen, "Distributed energy management for networked microgrids using online ADMM with regret," *IEEE Trans. Smart Grid*, vol. 9, no. 2, pp. 847–856, Mar. 2018.

[16] A. X. Sun, D. T. Phan, and S. Ghosh, "Fully decentralized AC optimal power flow algorithms," in *Proc. IEEE Power Energy Soc. Gen. Meeting*, Vancouver, BC, Canada, Jul. 2013, pp. 1–5.

[17] Y. Wang, S. Mao, and R. M. Nelms, "An online algorithm for optimal real-time energy distribution in the smart grid," *IEEE Trans. Emerg. Topics Comput.*, vol. 1, no. 1, pp. 10–21, Jul. 2013.

[18] N. Chen, A. Agarwal, A. Wierman, S. Barman, and L. L. H. Andrew, "Online convex optimization using predictions," *ACM Sigmetrics Perform. Eval. Rev.*, vol. 43, no. 1, pp. 191–204, Jun. 2015.

[19] S. Boyd, N. Parikh, E. Chu, B. Peleato, and J. Eckstein, "Distributed optimization and statistical learning via the alternating direction method of multipliers," *Found. Trends Mach. Learn.*, vol. 3, no. 1, pp. 1–122, Jan. 2011.

[20] Z. W. Wen, W. T. Yin, X. Liu, and Y. Zhang, "Introduction to compressive sensing and sparse optimization," *Oper. Res. Trans.*, vol. 16, no. 3, pp. 49–64, Sep. 2012.

[21] S. H. Low, "Convex relaxation of optimal power flow—Part I: Formulations and equivalence," *IEEE Trans. Control Netw. Syst.*, vol. 1, no. 1, pp. 15–27, Mar. 2014.

[22] X. Bai, H. Wei, K. Fujisawa, and Y. Wang, "Semidefinite programming for optimal power flow problems," *Int. J. Elect. Power Energy Syst.*, vol. 30, nos. 6–7, pp. 383–392, Jul.–Sep. 2008.

[23] Y. Huang and S. Mao, "On quality of usage provisioning for electricity scheduling in microgrids," *IEEE Syst. J.*, vol. 8, no. 2, pp. 619–628, Jun. 2014.

[24] Y. Wang, H. Zou, X. Chen, F. Zhang, and J. Chen, "Adaptive solar power forecasting based on machine learning methods," *MDPI Appl. Sci.*, vol. 8, no. 11, p. 2224, Nov. 2018.

[25] W. C. Davidon, "Variable metric method for minimization," *SIAM J. Optim.*, vol. 1, no. 1, pp. 1–17, Feb. 1991.

[26] S. Wright and J. Nocedal, *Numerical Optimization*. New York, NY, USA: Springer-Verlag, 1999.

[27] A. R. Malekpour and A. Pahwa, "Stochastic networked microgrid energy management with correlated wind generators," *IEEE Trans. Power Syst.*, vol. 32, no. 5, pp. 3681–3693, Sep. 2017.

[28] R. Palma-Behnke *et al.*, "A microgrid energy management system based on the rolling horizon strategy," *IEEE Trans. Smart Grid*, vol. 4, no. 2, pp. 996–1006, Jun. 2013.

[29] J. Silvente, G. M. Kopanos, E. N. Pistikopoulos, and A. Espuña, "A rolling horizon optimization framework for the simultaneous energy supply and demand planning in microgrids," *Appl. Energy*, vol. 155, pp. 485–501, Oct. 2015.

Hualei Zou (S'18) received the B.E. degree in electrical engineering and automation from the Nanjing University of Aeronautics and Astronautics (NUAA), Nanjing, China, in 2008, and the M.E. degree in power electronics and power drives from Jiangsu University, Zhenjiang, China, in 2011. She is currently pursuing the Ph.D. degree with the Department of Electrical Engineering, NUAA.

Her research interests include energy management in smart grid and microgrid, and optimization.

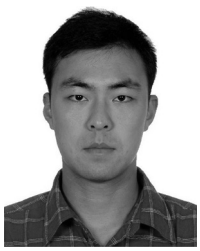

Yu Wang (S'13–M'17) received the B.S. and M.S. degrees in instrument and meter engineering from Southeast University, Nanjing, China, in 2008 and 2011, respectively, and the Ph.D. degree in electrical and computer engineering from Auburn University, Auburn, AL, USA, in 2015.

He is currently an Assistant Professor with the Department of Electrical Engineering, Nanjing University of Aeronautics and Astronautics, Nanjing. His research interests include smart grid, microgrid, renewable energy power forecasting, management, and optimization.

Shiwen Mao (S'99–M'04–SM'09–F'19) received the Ph.D. degree in electrical and computer engineering from Polytechnic University (currently, New York University Tandon School of Engineering), New York, NY, USA.

He was the McWane Associate Professor with Auburn University, Auburn, AL, USA, from 2012 to 2015, where he is currently the Samuel Ginn Distinguished Professor with the Department of Electrical and Computer Engineering, and the Director of the Wireless Engineering Research and Education Center. His research interests include wireless networks, multimedia communications, and smart grid.

Dr. Mao received the IEEE ComSoc TC-CSR Distinguished Technical Achievement Award in 2019, the IEEE ComSoc MMTC Distinguished Service Award in 2019, the Auburn University Creative Research & Scholarship Award in 2018, the 2017 IEEE ComSoc ITC Outstanding Service Award, the 2015 IEEE ComSoc TC-CSR Distinguished Service Award, the 2013 IEEE ComSoc MMTC Outstanding Leadership Award, and the NSF CAREER Award in 2010. He is a co-recipient of the 2018 IEEE ComSoc MMTC Best Journal Paper Award, the 2017 IEEE ComSoc MMTC Best Conference Paper Award, the Best Demo Award from IEEE SECON 2017, the Best Paper Awards from IEEE GLOBECOM 2019, 2016, and 2015, IEEE WCNC 2015, and IEEE ICC 2013, and the 2004 IEEE Communications Society Leonard G. Abraham Prize in the Field of Communications Systems. He is a Distinguished Speaker from 2018 to 2021 and was a Distinguished Lecturer from 2014 to 2018 of the IEEE Vehicular Technology Society. He is on the editorial board of the IEEE OPEN JOURNAL OF THE COMMUNICATIONS SOCIETY, the IEEE TRANSACTIONS ON NETWORK SCIENCE AND ENGINEERING, the IEEE TRANSACTIONS ON MOBILE COMPUTING, IEEE INTERNET OF THINGS JOURNAL, IEEE MULTIMEDIA, IEEE NETWORKING LETTERS, *IEEE/CIC China Communications*, and ACM GetMobile.

Fanghua Zhang received the B.S. degree in automation and electrical engineering from Jinan University, Jinan, China, in 1999, and the Ph.D. degree in electrical engineering from the Nanjing University of Aeronautics and Astronautics (NUAA), Nanjing, China, in 2004.

He joined the College of Automation Engineering, NUAA, in June 2004, as a Lecturer and became an Associate Professor in March 2006. His research focuses on dc–dc converter, high-performance aeronautical static inverter for aerospace applications, and power electronic systems stability and power quality.

Xin Chen (S'99–M'04) received the B.S. and Ph.D. degrees in electrical engineering from the Nanjing University of Aeronautics and Astronautics (NUAA), Nanjing, China, in 1996 and 2001, respectively.

From 2001 to 2003, he was a Chief Engineer with the Power Division of ZTE Corporation, Shenzhen, China. From 2010 to 2011, he was an Invited Researcher with the Rensselaer Polytechnic Institute, Troy, NY, USA. He is currently an Associate Professor with NUAA. His current research interests include power electronic converters, distributed generation, and microgrids.